SUPPLEMENTAL TABLE OF CONTENTS

Supplemental Table 1. Rat primers used for qRT-PCR

Gene Name	*Forward*	*Reverse*
Gapdh	TGCACCACCAACTGCTTAGC	GGCATGGACTGTGGTCATGA
Actn4	ACCATGCCTTTTCAGGAGCG	CTTCTGAGGCACACGGTCTT
Nphs1	CCACAGCGAGGCACTCCGTG	AGGATACGGTGCCGGGGACC
Nphs1	CCACAGCGAGGCACTCCGTG	AGGATACGGTGCCGGGGACC
Nebl	AGGAGCACCCGTCCTTCC	TAGGTCCTTAGATTTGCTGAATGCT

Supplemental Figure 1. Enrichment analyses for the top 52 consistently downregulated glomerular proteins in the transient rat puromycin aminonucleoside-induced nephropathy model. Proteomic hits were used to determine representation via the *EnrichR* suite within **(A)** gene ontology (GO) biological processes, **(B)** GO molecular function, **(C)** *ChEA* transcription factors, and **(D)** *MGI* mouse phenotype databases.

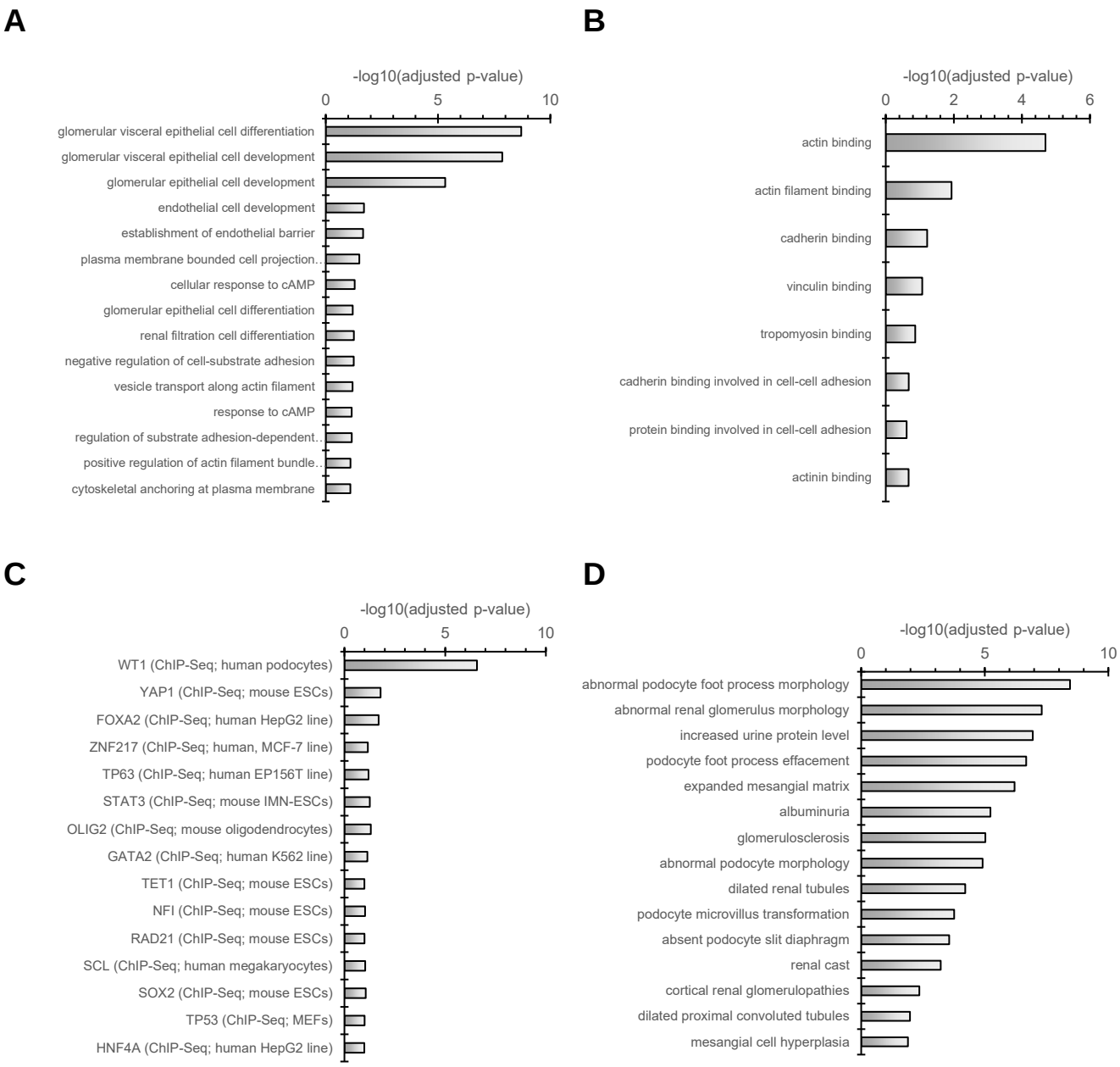

Supplemental Figure 2. Correlation between normalized nebulette expression levels as quantified by isobaric tagged proteomics and glomerular function as quantified by urine albumin/creatinine ratio.

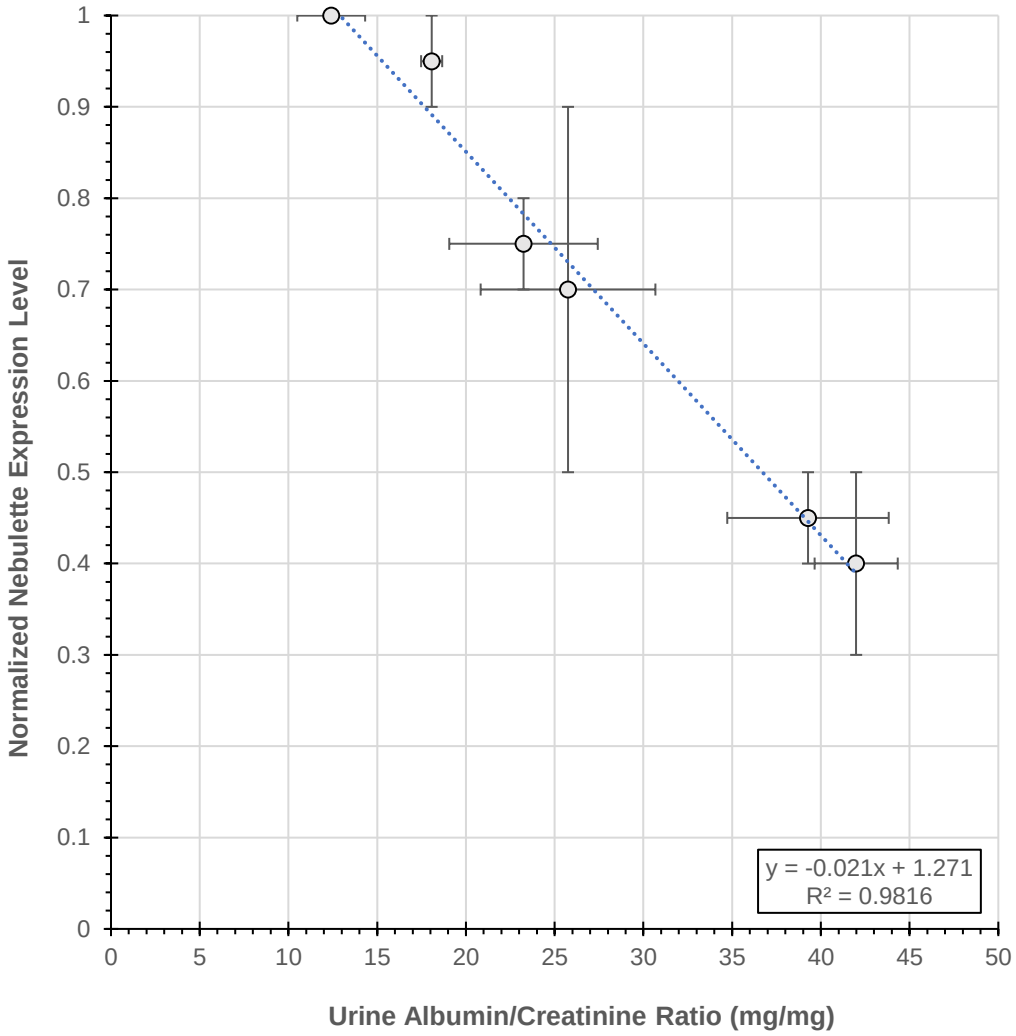

Supplemental Figure 3. Domains and the amino acid sequences of the two nebulette isoforms in the rat, and the mass spectrometry-detected peptides highlighted in yellow and cyan. We note that all the detected peptide spectra stem from the C-terminus region that is common between the two isoforms as shown in bold. None of the peptides unique to the first isoform are detected even though it is five times larger in size.

Nebulette (Isoform-1), Rattus Norvegicus (Uniprot ID : D4A164_RAT, 1015 AA)

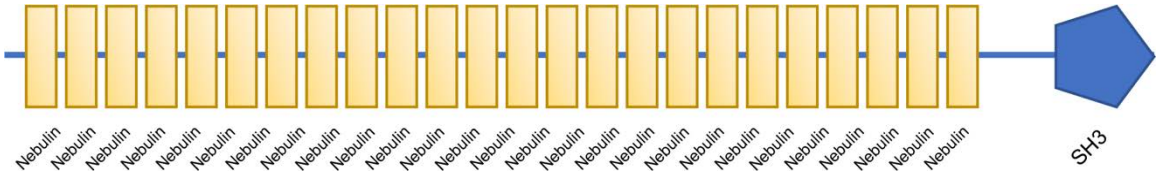

MKVPVSGDVKEETEEENVEEEEKPEDEVFLKPVVEDLSMELARKCTELISDIHYKEDYRKSKDKCTSVTDTP
TLNHVKNISAFISETKYKGTIKADLSNCLYKDMPATIDSVFAREVSQLQSEVAYKQKHEAEKGLSDYAHMKEP
PEVRHAMEVNRHQSNISYRKDVQGTHTYTAEMDRPDIKKATQISKIISNAEYKKGQGIVNKEPSVIGRPDFEH
AVEASKLSSQVKYKEKFDNEMKGKGHHYNPLGSASFRQHQLATVLASDVKYKKDVQTMHEPVSDLPNLLFL
DHALKASRMLSGWEYKKNFEENKGSYHFDAEAPEHLHHRGNATLQSQVKYREEYEKNKGKTMLDFVETPS
YQSSKEAQKMQSEKVYKEDFEKEIKGRSSLDLDKTPAFLHVKHISNLMREKEYKKDLENEIKGKGMELSSEV
LDIQRAKRASEMASEKEYKKDLELEIKGKGMQIDADTLEIQRVKRAAKIASEKDYKRDLETEIKGKGMQVSTD
TLDVQRAKRASEMASQKQYRKDLENEIKGKGMQVNVDIPDMLRAKRASEIYSQKKYKDEAEKMLSNYSTVA
VTPEIQRIKTTQQNISNVSYKEEVRAGTAVRNTPEIERVKKNQHNISSVKFEEGIKHATAISDPLELKRVTENQ
KDVINRFQYKEPTYKATPVTMTPEIERVRRNQEQLSAVKHKGELKQATSILDLPGLKRVRENQKTISNVYYK
GQLGRATALSVTPEMERVKKNQENISSVKYTQDHKQMKGRPCVILDTPALRHVKEAQNHVSM**VKYHEDFE**
KTKGRGFTPVVDDPVTERVRKNTQVVSDAAYKGVQPHVVEMDRRPGIIVDLKVWRTDPGSIFDIDPLEDNI
QSRSLHMLSEKASQYQSRLSRSHSGSTFGTGLGDDKSEISELYPSFSCCSEVTRPSDEGAPVLPGAYQQS
HSQGYGYMHQTSVSSVRSMQHSANLRTYRAMYDYSAQDEDEVSFRDGDYIVNVQPIDDGWMYGTVQRTG
RTGMLPANYIEFVN

LIM-nebulette (Isoform-2), Rattus Norvegicus (Uniprot ID: A0A146J2K6_RAT, 270 AA)

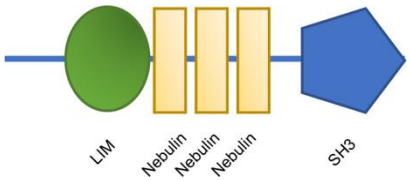

MNPQCARCGKVVYPTEKVNCLDKYWHKGCFHCEVCKMALNMNNYKGYEKKPYCNAHYPKQSFTTVADTP
ENLRLKQQSELQSQVKYKRDFEESRGRGFSIVTDTPELQRLKRTQEQISN**VKYHEDFEKTKGRGFTPVVDD**
PVTERVRKNTQVVSDAAYKGVQPHVVEMDRRPGIIVAPVLPGAYQQSHSQGYGYMHQTSVSSVRSMQHS
ANLRTYRAMYDYSAQDEDEVSFRDGDYIVNVQPIDDGWMYGTVQRTGRTGMLPANYIEFVN

Supplemental Figure 4. The epitopes for the antibodies used in the study as superimposed over the BLAST alignment performed by Uniprot Clustal Omega (version 1.2.4) on the two human proteins: nebulette isoform-1 (homo sapiens, NCBI ID: NP_006384.1, Uniprot ID: NEBL_HUMAN, O76041) and LIM-nebulette (homo sapiens, NCBI ID: NP_998734.1, Uniprot ID: O76041-2). The antibody for nebulette, which was used *only* for validation of knockout in the heart, targets an epitope (highlighted in green) that is conserved in the rat and mouse by ~90%. The antibody for LIM-nebulette, which has been used for most of the assays in this study, targets an internal epitope (highlighted in magenta) that is conserved in the rat and mouse by 100%. It has no overlap with nebulette isoform-1 or Lasp1.

```
O76041|NEBL_HUMAN    MRVPVFEDIKDETEEEKIGEEENEEDQVFYKPVIEDLSMELARKCTELISDIRYKEEFKK 60
O76041-2|NEBL_HUMAN  ------------------------------------------------------------

O76041|NEBL_HUMAN    SKDKCTFVTDSPMLNHVKNIGAFISEAKYKGTIKADLSNSLYKRMPATIDSVFAGEVTQL 120
O76041-2|NEBL_HUMAN  ------------------------------------------------------------

O76041|NEBL_HUMAN    QSEVAYKQKHDAAKGFSDYAHMKEPPEVKHAMEVNKHQSNISYRKDVQDTHTYSAELDRP 180
O76041-2|NEBL_HUMAN  ------------------------------------------------------------

O76041|NEBL_HUMAN    DIKMATQISKIISNAEYKKGQGIMNKEPAVIGRPDFEHAVEASKLSSQIKYKEKFDNEMK 240
O76041-2|NEBL_HUMAN  ------------------------------------------------------------

O76041|NEBL_HUMAN    DKKHHYNPLESASFRQNQLAATLASNVKYKKDIQNMHDPVSDLPNLLFLDHVLKASKMLS 300
O76041-2|NEBL_HUMAN  ------------------------------------------------------------

O76041|NEBL_HUMAN    GREYKKLFEENKGMYHFDADAVEHLHHKGNAVLQSQVKYKEEYEKNKGKPMLEFVETPSY 360
O76041-2|NEBL_HUMAN  ------------------------------------------------------------

O76041|NEBL_HUMAN    QASKEAQKMQSEKVYKEDFEKEIKGRSSLDLDKTPEFLHVKYITNLLREKEYKKDLENEI 420
O76041-2|NEBL_HUMAN  ------------------------------------------------------------

O76041|NEBL_HUMAN    KGKGMELNSEVLDIQRAKRASEMASEKEYKKDLESIIKGKGMQAGTDTLEMQHAKKAAEI 480
O76041-2|NEBL_HUMAN  ------------------------------------------------------------

O76041|NEBL_HUMAN    ASEKDYKRDLETEIKGKGMQVSTDTLDVQRAKKASEMASQKQYKKDLENEIKGKGMQVSM 540
O76041-2|NEBL_HUMAN  ------------------------------------------------------------

O76041|NEBL_HUMAN    DIPDILRAKRTSEIYSQRKYKDEAEKMLSNYSTIADTPEIQRIKTTQQNISAVFYKKEVG 600
O76041-2|NEBL_HUMAN  ------------------------------------------------------------

O76041|NEBL_HUMAN    AGTAVKDSPEIERVKKNQQNISSVKYKEEIKHATAISDPPELKRVKENQKNISNLQYKEQ 660
O76041-2|NEBL_HUMAN  ------------------------------------------------------------

O76041|NEBL_HUMAN    NYKATPVSMTPEIERVRRNQEQLSAVKYK-GELQRGTAISDPPELKRAKEN-----QKNI 714
O76041-2|NEBL_HUMAN  --------MNPQCARCGKVVYPTEKVNCLDKYWHKGCFHCEVCKMALNMNNYKGYEKKPY 52
                           *.*:  *  :     . *:      ::*   .:  ::    :*     :*
O76041|NEBL_HUMAN    SNVYYRGQLGRATTLSVTPEMERVKKNQENISSVKYTQDHKQMKGRP-SLILDTPAMRHV 773
O76041-2|NEBL_HUMAN  CNAHYP--KQSFTTVADTPENLRLKQQSELQSQVKYKRDFEESKGRGFSIVTDTPELQRL 110
                     .*.:*       **:: ***  *:*::.*  *.***.:*.:: ***  *:: *** ::::
O76041|NEBL_HUMAN    KEAQNHISMVKYHEDFEKTKGRGFTPVVDDPVTERVRKNTQVVSDAAYKGVHPHIVEMDR 833
O76041-2|NEBL_HUMAN  KRTQEQISNVKYHEDFEKTKGRGFTPVVDDPVTERVRKNTQVVSDAAYKGVHPHIVEMDR 170
                     *.:*::** **************************************************
O76041|NEBL_HUMAN    RPGIIVDLKVWRTDPGSIFDLDPLEDNIQSRSLHMLSEKASHYRRHWSRSHSSSTFGTGL 893
O76041-2|NEBL_HUMAN  RPGIIV------------------------------------------------------ 176
                     ******
O76041|NEBL_HUMAN    GDDRSEISEIYPSFSCCSEVTRPSDEGAPVLPGAYQQSHSQGYGYMHQTSVSSMRSMQHS 953
O76041-2|NEBL_HUMAN  -------------------------APVLPGAYQQSHSQGYGYMHQTSVSSMRSMQHS 209
                                              ********************************
O76041|NEBL_HUMAN    PNLRTYRAMYDYSAQDEDEVSFRDGDYIVNVQPIDDGWMYGTVQRTGRTGMLPANYIEFV 1013
O76041-2|NEBL_HUMAN  PNLRTYRAMYDYSAQDEDEVSFRDGDYIVNVQPIDDGWMYGTVQRTGRTGMLPANYIEFV 269
                     ************************************************************

O76041|NEBL_HUMAN    N 1014
O76041-2|NEBL_HUMAN  N 270
                     *
```

Supplemental Figure 5. Analysis of *NEBL* expression in public databases. **(A)** Unsupervised clustering of 4,259 single nuclei that has identified six distinct cell types in human adult kidney. These types include three tubular cell types of proximal tubule (PT), loop of Henle (LH), and distal tubule (DT); two collecting duct (CD) cell types of principal cells (PC) and intercalated cells (IC); and one podocyte population (P). **(B)** Unsupervised clustering of 4,524 single-nuclear RNA sequencing of adult human kidney that has identified 17 distinct cell types in human adult kidney including 11 tubular cell types, podocytes, mesangium, endothelial cells, and macrophages. Superimposed over the tSNE plots are the expression levels of *NEBL*, *NPHS1*, *NPHS2*, and *ACTN4* transcripts.

A

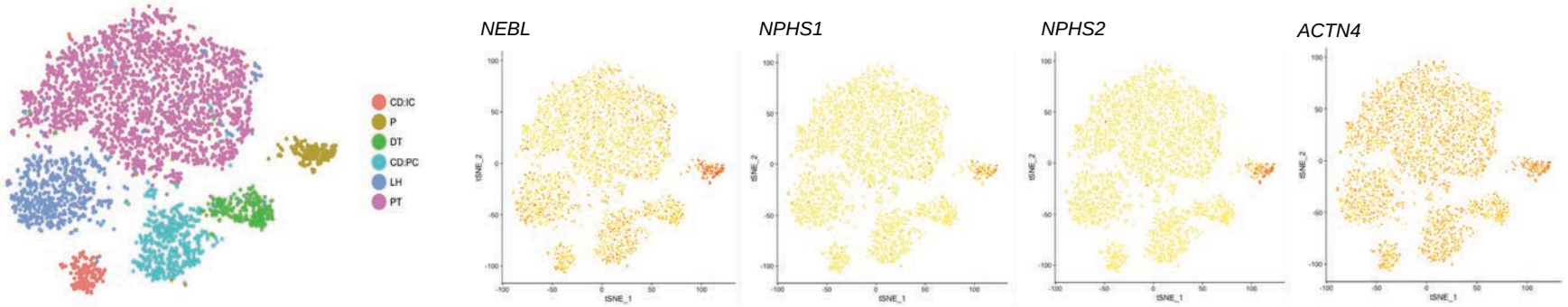

from Wu and Malone *et al.* J Am Soc Neph 2018 (Human Adult Kidney, Epithelial)

B

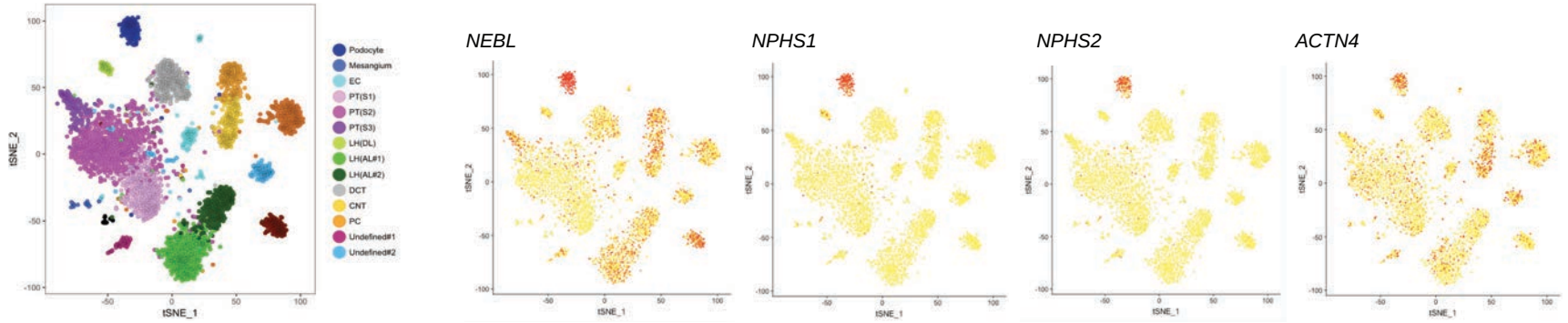

from Wu and Uchimura *et al.* Cell Stem Cell 2018 (Human Adult Kidney, Total)

Supplemental Figure 6. Super resolution imaging of human glomeruli. **(A)** Stimulated emission-depletion (STED) imaging at 100X and **(B)** Zeiss Airyscan laser scanning confocal imaging at 63X showing expression of LIM-nebulette (magenta) and actinin-4 (cyan) localizing to visceral epithelial processes.

A

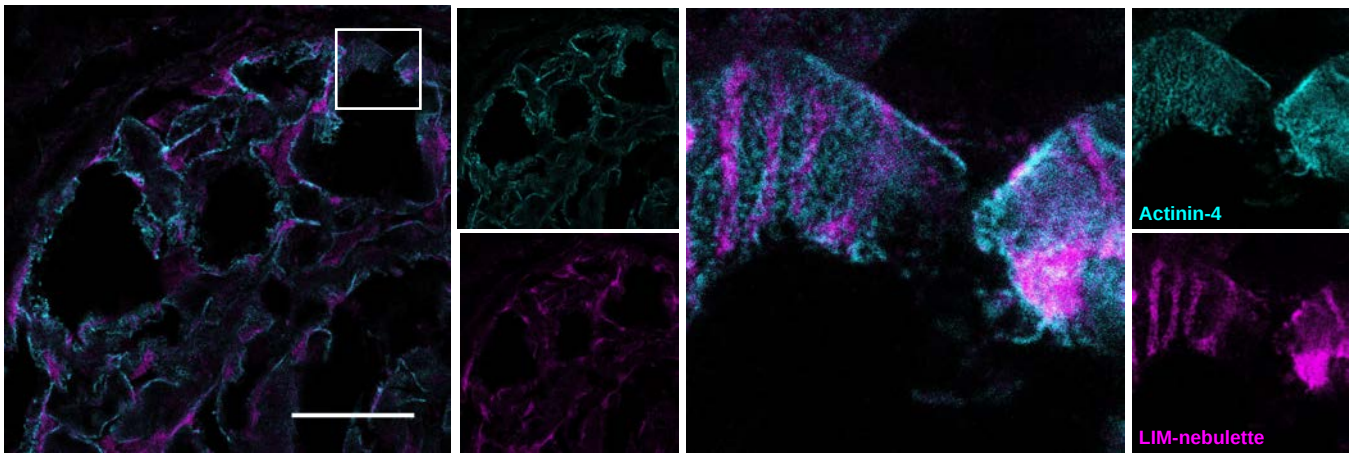

B

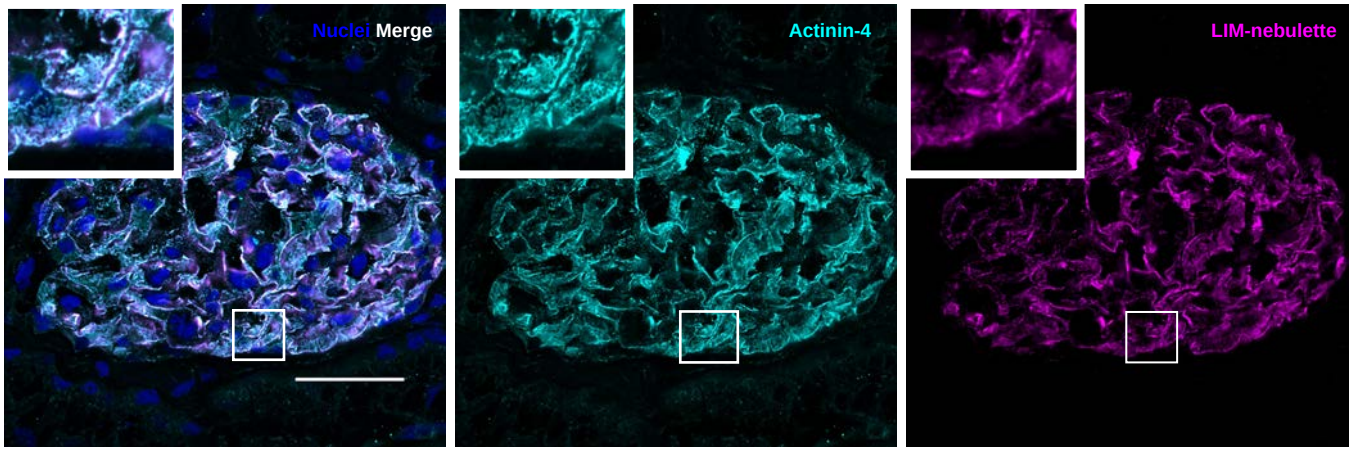

Supplemental Figure 7. Histopathological assessment of wild type (WT) and nebulette knockout (KO) mice using hematoxylin and eosin (H&E), Periodic acid-Schaff (PAS), Masson's trichorome (MASSON) and Picrosirius red (SRED) staining.

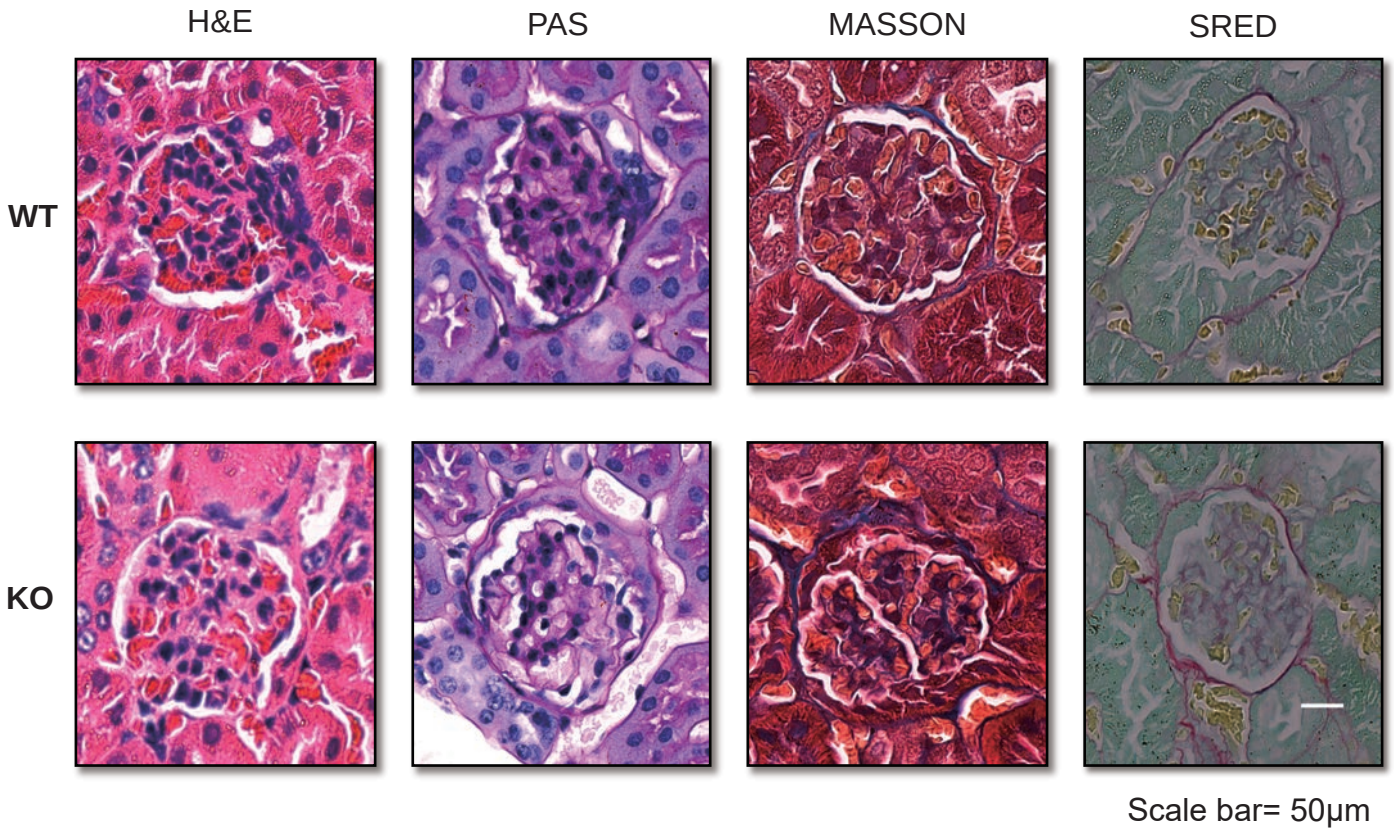

Supplemental Figure 8. Visual comparison of albuminuria between wild type (WT) and nebulette knockout (KO) mice injected with single dose of Adriamycin (ADR). Urine was collected at basline (W0), and weekly for four weeks (W1, W2, W3, W4). SDS-PAGE Coomasie brilliant blue staining of bovine serum albumin (BSA) standards and urine samples from WT and KO mice.

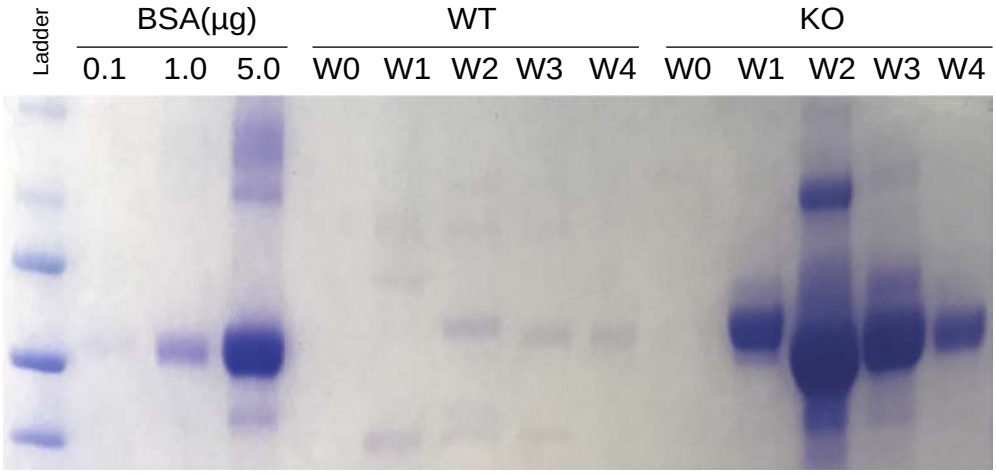

Supplemental Figure 9. Freshly isolated mouse primary podocytes from **(A)** wild type (WT) and **(B)** nebulette knockout (KO) animals showing expression of paxillin, F-actin, Wilm's tumor 1 (WT1), and nuclei (Hoechst). Scale bars = 50 µm.

A

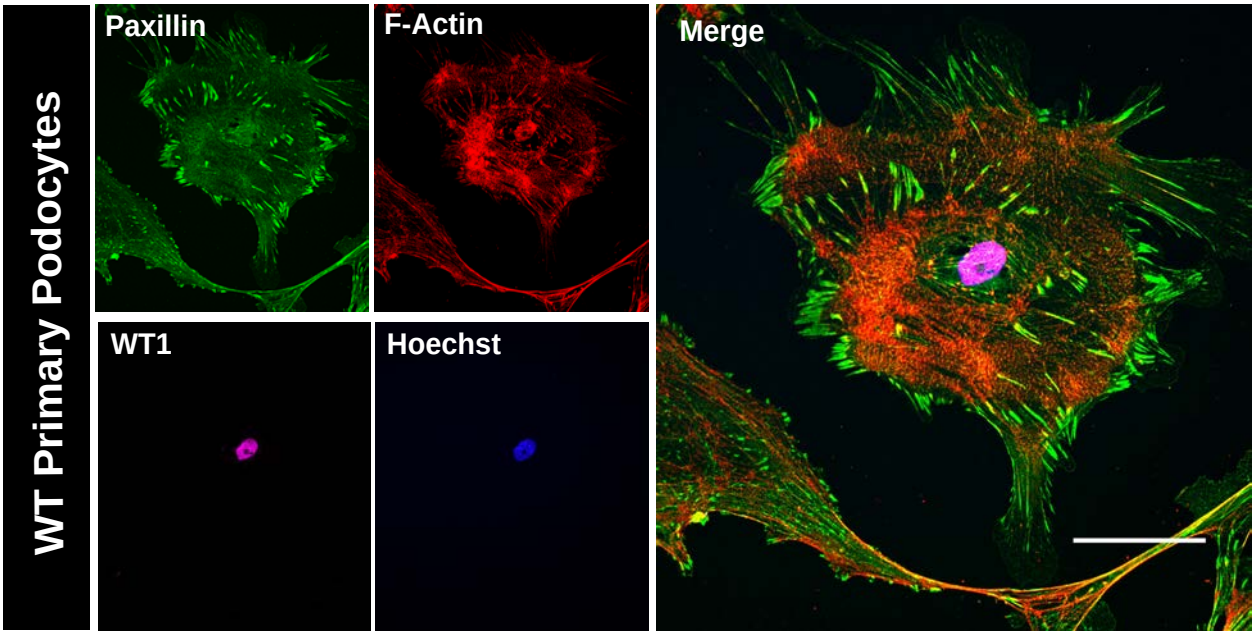

B

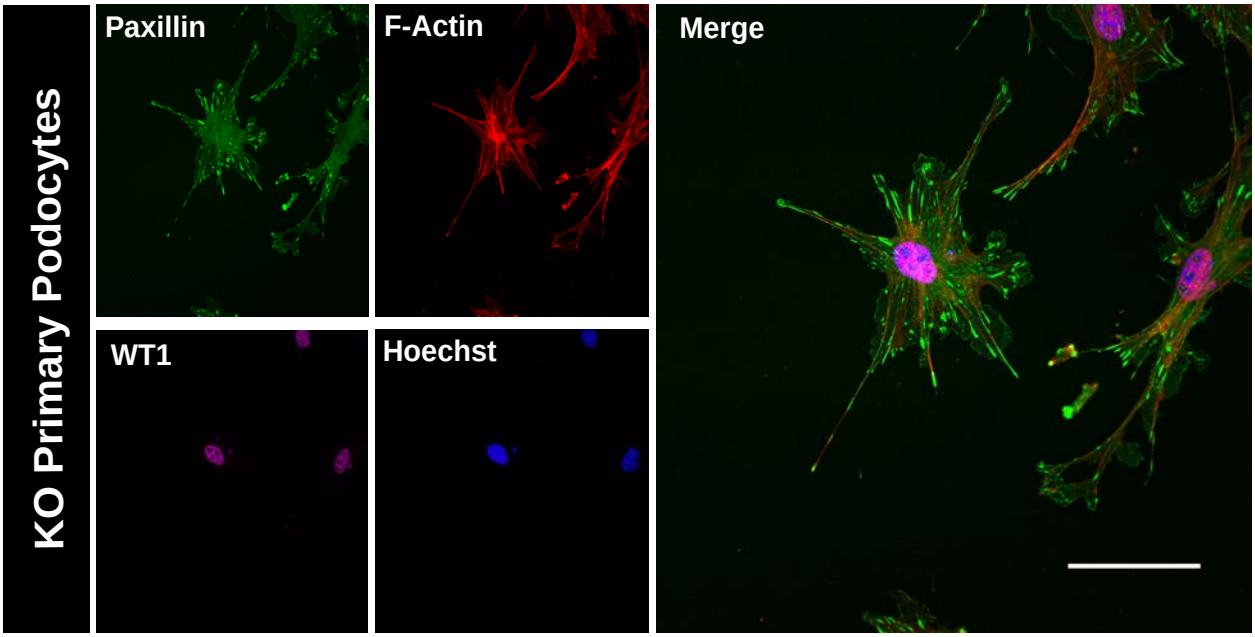

Supplemental Figure 10. Expression of LIM-nebulette in immortalized human podocyte cell line **(A)** as assessed by western blotting before (33ºC) and after (37ºC) differentiation for 10 days and quantified. **(B)** Spatial distribution of LIM-nebulette (magenta), actinin-4 (cyan), F-actin (red) and nuclei (blue) in the immortalized human podocyte cell line differentiated for 10 days at 37ºC. Scale bar = 50 µm.

A

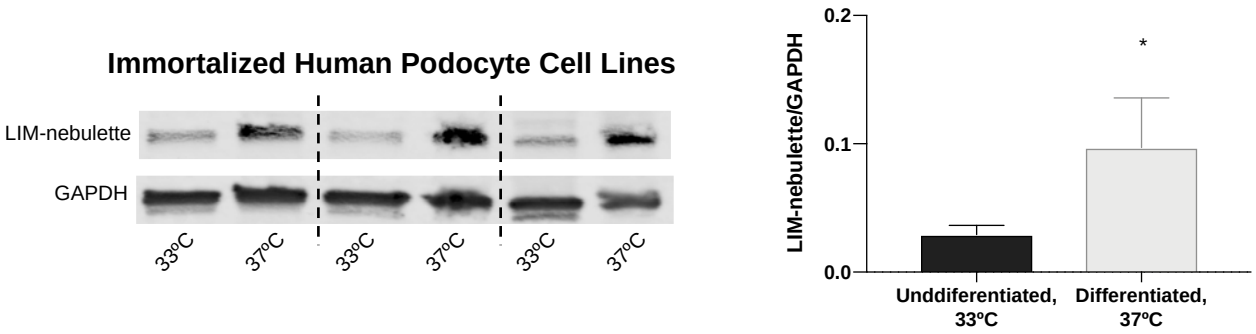

B

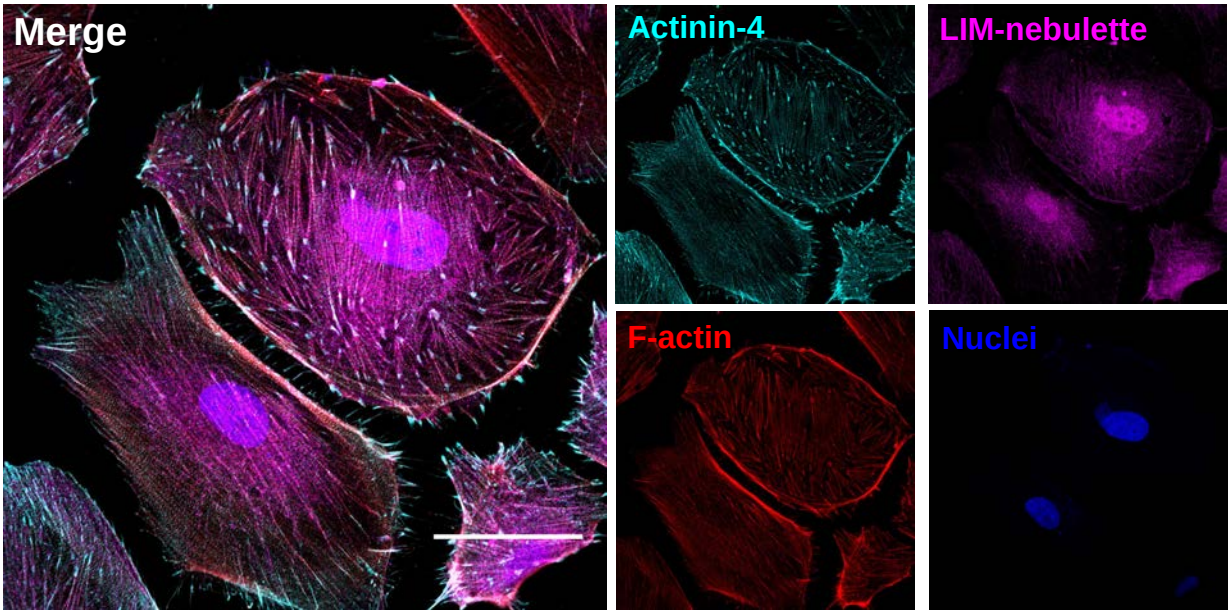

Supplemental Figure 11. Morphological comparison of arborization in freshly isolated mouse primary podocytes (left), human induced pluripotent stem cell (hiPSC)-derived podocytes (middle), and immortalized human podocyte cell line (right) under phase contrast bright field at 40X magnification. Scale bars = 100 µm.

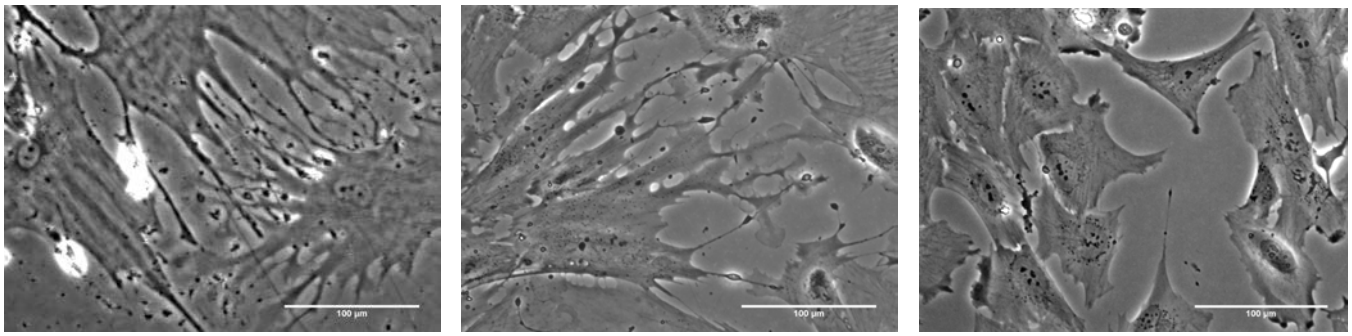

Mouse primary podocytes **hiPSC-derived podocytes** **Immortalized human podocytes cell line**

Supplemental Figure 12. Expression of nebulette in immortalized human podocyte cell line expressing scrambled or PAN-nebulette shRNA was assessed using Western blotting and quantified.

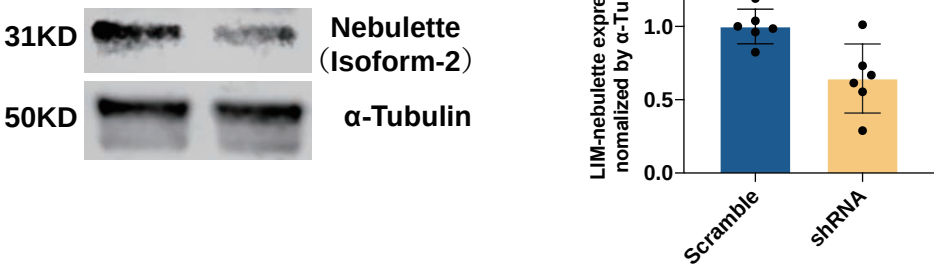

Supplemental Figure 13. Spatial distribution of subcellular elasticity of primary podocytes isolated from *Nebl*$^{+/+}$ (WT) or *Nebl*$^{-/-}$ (KO) mice. Cells were cultured on 50-mm type-I collagen coated dishes for 48 hours and probed using a standard pyramidal tip over a 6 x 6 perinuclear indentation array on an Asylum MFP-3D atomic force microscope (AFM) at 37ºC. Podocytes from KO animals had a significantly lower elastic modulus (**p = 0.0013; repeated measures ANOVA, n = 108). Median ± interquartile range of apparent elastic modulus for WT cells was 18.3 ± 11.9 kPa versus 11.3 ± 3.5 kPa in KO cells. AFM indentation rate was 10 µm/sec. Probed cellular volumes were 20 x 20 x 5 µm.

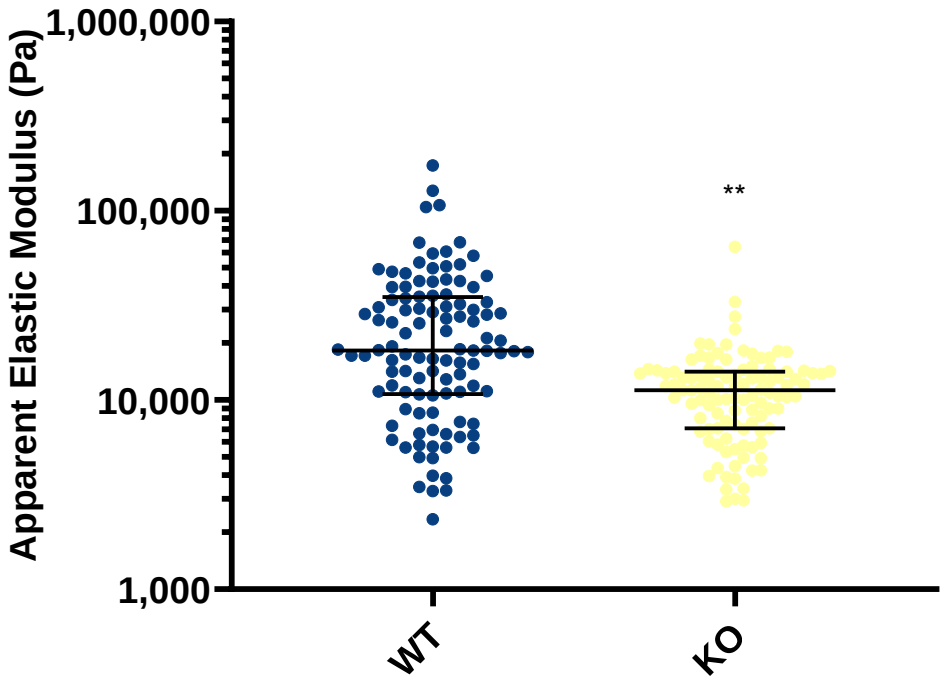

Supplemental Figure 14. Changes in spatial distribution of LIM-nebulette (magenta) in differentiated immortalized human podocytes upon exposure to F-actin (Cytochalasin D and Latrunculin B) or vimentin (Arylquin-1 and Withaferin A) disruptors. Representative immunofluorescence images were taken at 63X using Zeiss Airyscan super-resolution confocal microscope.Scale bars = 25 µm.